An Elastic–Viscous–Plastic Model for Sea Ice Dynamics

E. C. HUNKE

Group T-3 and the Center for Nonlinear Studies, Theoretical Division, Los Alamos National Laboratory, Los Alamos, New Mexico

J. K. DUKOWICZ

Group T-3, Theoretical Division, Los Alamos National Laboratory, Los Alamos, New Mexico

(Manuscript received 2 September 1996, in final form 22 January 1997)

ABSTRACT

The standard model for sea ice dynamics treats the ice pack as a visco–plastic material that flows plastically under typical stress conditions but behaves as a linear viscous fluid where strain rates are small and the ice becomes nearly rigid. Because of large viscosities in these regions, implicit numerical methods are necessary for time steps larger than a few seconds. Current solution methods for these equations use iterative relaxation methods, which are time consuming, scale poorly with mesh resolution, and are not well adapted to parallel computation. To remedy this, the authors developed and tested two separate methods. First, by demonstrating that the viscous–plastic rheology can be represented by a symmetric, negative definite matrix operator, the much faster and better behaved preconditioned conjugate gradient method was implemented. Second, realizing that only the response of the ice on timescales associated with wind forcing need be accurately resolved, the model was modified so that it reduces to the viscous–plastic model at these timescales, whereas at shorter timescales the adjustment process takes place by a numerically more efficient elastic wave mechanism. This modification leads to a fully explicit numerical scheme that further improves the model's computational efficiency and is a great advantage for implementations on parallel machines.

Furthermore, it is observed that the standard viscous–plastic model has poor dynamic response to forcing on a daily timescale, given the standard time step (1 day) used by the ice modeling community. In contrast, the explicit discretization of the elastic wave mechanism allows the elastic–viscous–plastic model to capture the ice response to variations in the imposed stress more accurately. Thus, the elastic–viscous–plastic model provides more accurate results for shorter timescales associated with physical forcing, reproduces viscous–plastic model behavior on longer timescales, and is computationally more efficient overall.

1. Introduction

A model of sea ice dynamics predicts the movement of the ice pack based on winds, ocean currents, and a model of the material strength of the ice. Nonuniform motion of the ice is responsible for the thickness and extent of the ice pack, which in turn influences the exchange of energy between the atmosphere and polar oceans. The dynamic characteristics of sea ice thereby play an essential role in climate-related processes of the ocean and atmosphere.

Many models have been developed to describe the ice dynamics. Some early studies focused on free drift descriptions with no ice interaction (Felzenbaum 1961; Bryan et al. 1975; Manabe et al. 1979; Parkinson and Washington 1979); others included more complex sea ice rheologies, treating the ice as a Newtonian viscous fluid (Campbell 1965), a linear viscous fluid (Hibler 1974; Hibler and Tucker 1979), or a plastic material. The Arctic Ice Dynamics Joint Experiment (AIDJEX) in the 1970s proposed an elastic–plastic rheology for the sea ice pack (Coon et al. 1974), and several other nonlinear plastic rheologies have been studied since then (e.g., Pritchard et al. 1977; Flato and Hibler 1992; Ip et al. 1991). A nonlinear viscous–plastic (VP) rheology proposed by Hibler (1979) has become the standard sea ice dynamics model and the basis for many recent sea ice studies.

The VP model suffers from numerical difficulties related to the enormous range of effective viscosities present in the model and requires large computational resources that become particularly cumbersome when the model is coupled to an ocean or atmophere model (Hibler and Bryan 1987; Oberhuber 1993a,b). To avoid the stringent time step restriction for stability of an explicit numerical scheme in regions where the ice is relatively rigid, the model equations are typically solved with implicit methods such as successive overrelaxation (Hibler 1979) and line relaxation (Oberhuber 1993a; Holland et

Corresponding author address: Dr. Elizabeth C. Hunke, Theoretical Division, Group T-3, Los Alamos National Laboratory, Mail Stop B216, Los Alamos, NM 87545.
E-mail: eclare@lanl.gov

al. 1993). However, these methods suffer from poor convergence characteristics as the mesh resolution is increased. Attempts to overcome the inherent problems of the model have included improved numerical methods as well as simplifications of the model itself. As part of this paper, we present a more efficient implicit numerical method for solving the VP model equations that uses preconditioned conjugate gradients.

Simpler versions of the VP model, such as free drift descriptions with no ice interaction and cavitating fluid models in which the ice has no resistance to shear forces (Nikiforov et al. 1967; Flato and Hibler 1989, 1992), are more tractable numerically, but the model behavior is sensitive to these simplifications (Holland et al. 1993). Likewise, simulations with more complicated rheologies than the standard elliptical yield curve (Hibler 1979), such as teardrop (Coon et al. 1974), sine wave lens (Bratchie 1984), Mohr–Coulomb, and square (Ip et al. 1991) shapes, show that the rheology can have a significant effect on long-term simulations of ice drift (Ip et al. 1991). Since an ice model need only simulate a visco–plastic material at timescales on the order of those imposed by wind forcing (days), we also present a modification of the model, the addition of elastic behavior, that realizes significant gains in numerical efficiency, reduces to the original VP model behavior at long timescales, and is more accurate for transients. Our model avoids the complexities of the early elastic–plastic models (Pritchard 1975; Colony and Pritchard 1975) because the elastic-like behavior is not intended to be physically realistic and is introduced for numerical expediency.

The VP model also suffers from inaccuracies in calculating transient behavior. For example, given daily time steps, the VP model behavior is acceptable only for surface stresses that vary on the order of a week or more. Hibler (1979) states that several time steps are needed between changes in the forcing (he uses 8-day averaged winds with a 1-day time step), and more recently, Stössel et al. (1994) have noted that the sea ice components of some ice–ocean coupled models are slow to converge, especially under daily forcing. The VP numerical model does produce correct transient behavior if the time step is taken sufficiently small, on the order of minutes for 1-day forcing timescales. Our implementation of the elastic–viscous–plastic (EVP) model is more accurate in resolving transients, even using relatively large time steps, and therefore will produce more accurate ice behavior.

The VP ice dynamics model is not well suited to parallel architectures. Implicit methods required for larger time steps typically entail a great deal of communication between processors, making parallel computation less attractive. Therefore, explicit models are generally preferable for parallel implementations. Ip et al. (1991) optimized the VP model for multiprocessor computers using an explicit, Euler time-stepping scheme, but stability requirements of the numerical method severely limited the time step. The new EVP model presented in this paper permits a fully explicit implementation with an acceptably long time step. Its efficiency is compared with three methods of solving the viscous–plastic equations: the preconditioned conjugate gradient method and two relaxation schemes (Hibler 1979; Zhang and Hibler 1996).

The present work is part of an effort to develop a computationally efficient sea ice component for a fully coupled atmosphere–ice–ocean global climate model. The sea ice model, which also includes thermodynamic and transport components, is designed to be compatible with the Parallel Ocean Program (POP), an ocean circulation model developed at Los Alamos National Laboratory for use on massively parallel computers (Smith et al. 1992; Dukowicz et al. 1993, 1994).

2. The ice dynamics model

a. Viscous–plastic model equations

Pack ice typically consists of rigid plates, which may drift freely in areas of relatively open water or be closely packed together in regions of high ice concentration. Although individual ice floes range from tens of meters to several kilometers across, the ice pack is considered to be a highly fractured two-dimensional continuum, to make modeling it tractable (Pritchard 1975; Rothrock 1975b; Hibler 1980; Gray and Morland 1994).

The force balance per unit area in the ice pack is given by a two-dimensional momentum equation (Hibler 1979), obtained by integrating the 3D equation through the thickness of the ice in the vertical direction:

$$m\frac{\partial u_i}{\partial t} = \frac{\partial \sigma_{ij}}{\partial x_j} + \tau_{ai} + \tau_{wi} + \varepsilon_{ij3} m f u_j - mg\frac{\partial H_o}{\partial x_i}, \quad (1)$$

where $\boldsymbol{\tau}_a = (\tau_{ai}, \tau_{aj})$ and $\boldsymbol{\tau}_w = (\tau_{wi}, \tau_{wj})$ are wind and ocean stresses, respectively, assumed to be of the form

$$\boldsymbol{\tau}_a = c_a \rho_a |\mathbf{U}_a| (\mathbf{U}_a \cos\phi + \mathbf{k} \times \mathbf{U}_a \sin\phi),$$

$$\boldsymbol{\tau}_w = c_w \rho_w |\mathbf{U}_w - \mathbf{u}| [(\mathbf{U}_w - \mathbf{u})\cos\theta + \mathbf{k} \times (\mathbf{U}_w - \mathbf{u})\sin\theta]. \quad (2)$$

The strength of the ice is represented by the internal stress tensor σ_{ij}. Definitions of the other variables and constants are given in Tables 1 and 2.

There has been a great deal of disagreement about the relative importance of the various terms in (1) (Parkinson and Washington 1979). The primary components are the air and water stresses, Coriolis force, and ice interaction effects (Hibler 1986); the most predominant of these is wind stress (Coon 1980). Rothrock (1975a) demonstrated through scale analyses that the acceleration term is three orders of magnitude smaller than the stress terms. In contrast to Hibler (1979) and following Oberhuber (1993a), we neglect nonlinear advection, which is at least an order of magnitude smaller than the acceleration term. The ice interaction term is essential in balancing the stresses in much of the ice field (Hibler

TABLE 1. Constants and parameters used in the dynamics equations.

c^*		20
c_a	air drag coefficient	
c_w	ocean drag coefficient	0.0055
δ_{ij}	Kronecker delta[a]	
ε_{ijk}	alternating tensor[b]	
e	yield curve axis ratio	2
g	gravitational acceleration	
H_o	sea surface height	
$\hat{k}$	vertical unit vector	
P^*		2.75×10^5 dyn cm^{-2}
ρ_a	air density	
ρ_i	sea ice density	0.91 g cm^{-3}
ρ_s	snow density	0.33 g cm^{-3}
ρ_w	seawater density	1.03 g cm^{-3}
θ	water turning angle	25°
ϕ	air turning angle	

[a] $\delta_{ij} = 1$ if $i = j$ and 0 if $i \neq j$.
[b] $\varepsilon_{ijk} = 0$ if any two indices are the same, 1 if the indices are in cyclical order, and -1 otherwise.

TABLE 2. Definitions of other symbols used in the dynamics equations, and their interdependencies.

	Variable quantities	Interdependence
c	compactness	$\mathbf{u}$
E	Young's modulus	c, H
$\dot{\epsilon}_{ij}$	strain rate tensor	$\mathbf{u}$
f	Coriolis parameter	
h	thickness of thin ice	$\mathbf{u}$
h_s	snow depth on thin ice	$\mathbf{u}$
H	thickness of thick ice	$\mathbf{u}$
H_s	snow depth on thick ice	$\mathbf{u}$
m	mass per unit area	c, H, H_s, h, h_s
P	pressure	c, H
η	shear viscosity	P, $\dot{\epsilon}_{ij}$
ζ	bulk viscosity	P, $\dot{\epsilon}_{ij}$
σ_{ij}	stress tensor	η, ζ, P, $\dot{\epsilon}_{ij}$
$\boldsymbol{\tau}_a$	wind stress	
$\boldsymbol{\tau}_w$	ocean stress	$\mathbf{u}$
$\mathbf{u}$	ice velocity	σ_{ij}, $\boldsymbol{\tau}_w$, m
$\mathbf{U}_a$	geostrophic wind	
$\mathbf{U}_w$	geostrophic ocean current	

1979; Parkinson and Washington 1979; Coon 1980; Hibler 1986), and although they are smaller in magnitude, current and tilt effects are significant over long periods of time (Hibler 1986; Warn-Varnas et al. 1991).

The momentum equation must be consistent for any combination of ice and open water in a grid cell. Our particular model differentiates between thick and thin ice and tracks ice concentration with compactness, c, the fractional area of the cell covered with thick ice. When $c = 0$, there is no thick ice ($H = 0$), and there may be either thin ice ($h > 0$) or open water ($h = 0$). The mass m in (1) is the total mass of ice and snow per unit area, corresponding to $\int_0^H \rho\, dz$:

$$m = \rho_i[cH + (1 - c)h] + \rho_s[cH_s + (1 - c)h_s]. \quad (3)$$

Thin ice is assumed to have no strength, so that the internal stress tensor is nonzero only for thick ice. Since the surface stress terms $\boldsymbol{\tau}_{ai}$ and $\boldsymbol{\tau}_{wi}$ apply over the entire area, we see that thin ice in a cell that does not contain thick ice essentially exists in free drift, given by the momentum equation without ice interaction. In the special case when there is only open water, $m = 0$ and the ''ice'' velocity is that of the interface between atmosphere and ocean, calculated with $\boldsymbol{\tau}_a + \boldsymbol{\tau}_w = 0$.

The viscous–plastic rheology proposed by Hibler (1979) is given by a constitutive law that relates the internal ice stress σ_{ij} and the rates of strain $\dot{\epsilon}_{ij}$ through an internal ice pressure P and nonlinear bulk and shear viscosities, ζ and η, such that the principal components of stress lie on an elliptical yield curve with the ratio of major to minor axes e equal to 2. The constitutive law is given by

$$\sigma_{ij} = 2\eta\dot{\epsilon}_{ij} + (\zeta - \eta)\dot{\epsilon}_{kk}\delta_{ij} - P\delta_{ij}/2, \quad (4)$$

where

$$\dot{\epsilon}_{ij} = \frac{1}{2}\left(\frac{\partial u_i}{\partial x_j} + \frac{\partial u_j}{\partial x_i}\right). \quad (5)$$

Alternatively, this can be rewritten in the form

$$\frac{1}{2\eta}\sigma_{ij} + \frac{\eta - \zeta}{4\eta\zeta}\sigma_{kk}\delta_{ij} + \frac{P}{4\zeta}\delta_{ij} = \dot{\epsilon}_{ij}, \quad (6)$$

which will be useful to us later. This rheology allows the ice pack to diverge with little or no stress, yet resist compression and shearing motion under convergent conditions.

The pressure P, a measure of ice strength, depends on both thickness and compactness: $P = P^*cHe\ \exp[-c^*(1 - c)]$, where P^* and c^* are constants given in Table 1. This definition of P is equivalent to the standard formulation of Hibler (1979), because cH is approximately the same as his ''equivalent ice thickness'' h.

The viscosities increase with pressure and with decreasing strain rates:

$$\zeta = \frac{P}{2\Delta}, \quad (7)$$

$$\eta = \frac{P}{2\Delta e^2}, \quad (8)$$

$$\Delta = [(\dot{\epsilon}_{11}^2 + \dot{\epsilon}_{22}^2)(1 + e^{-2}) + 4e^{-2}\dot{\epsilon}_{12}^2 + 2\dot{\epsilon}_{11}\dot{\epsilon}_{22}(1 - e^{-2})]^{1/2}. \quad (9)$$

These parameters represent an idealized visco–plastic material whose effective viscosities become infinite in the limit of zero strain rate. Hibler (1979) chose to regularize this behavior by bounding the viscosities when the rates of strain are small and the ice pack moves as an essentially rigid solid; the limiting viscosities are set to large, constant values so that the ice pack is treated as a linear viscous fluid undergoing very slow creep. The maximum value for ζ is $2.5 \times 10^8\ P$ g s^{-1}; η is

similarly bounded through equations (7) and (8). He also set minimum values to provide against nonlinear instabilities, with $\zeta_{\min} = 4 \times 10^{11}$ g s^{-1}. For a sufficiently small value of c, $\zeta_{\max} < \zeta_{\min}$, in which case $\zeta = \zeta_{\min}$. For a general account of constitutive laws for sea ice, see Hibler (1986).

Equations (1), (2), (5), and (6) may be combined as follows:

$$m\partial_t u = \partial_x[(\eta + \zeta)\partial_x u] + \partial_y(\eta\partial_y u) + \partial_x[(\zeta - \eta)\partial_y v] + \partial_y(\eta\partial_x v) - \partial_x P/2 + c'[(U_w - u)\cos\theta - (V_w - v)\sin\theta] + \tau_{ai} + mfv - mg\partial_x H_o, \quad (10)$$

$$m\partial_t v = \partial_y[(\eta + \zeta)\partial_y v] + \partial_x(\eta\partial_x v) + \partial_y[(\zeta - \eta)\partial_x u] + \partial_x(\eta\partial_y u) - \partial_y P/2 + c'[(V_w - v)\cos\theta + (U_w - u)\sin\theta] + \tau_{aj} - mfu - mg\partial_y H_o, \quad (11)$$

where $c' = \rho_w C_w|\mathbf{U}_w - \mathbf{u}|$.

b. Motivation for alternative methods

Most sea ice models, starting with the models developed for the AIDJEX project, agree on a visco–plastic rheology at normal levels of strain rate, differing perhaps in the shape of the yield curve. The ideal visco–plastic rheology, however, becomes singular as the strain rate approaches zero. The AIDJEX model (Coon et al. 1974; Pritchard 1975) regularized this behavior by adopting a rheology that converts to that of an elastic material at small strain rates (an ''elastic–plastic'' rheology). It is important to realize that such an elastic rheology is physically realistic for ice only at a laboratory scale, but at geophysical scales there is no reason to prefer the elastic regularization to any other closure that ensures that the ice pack behaves as a rigid slab in the singular, small strain rate regime. Unfortunately, the AIDJEX model took the limiting elastic behavior quite literally (Pritchard 1975; Colony and Pritchard 1975), needlessly introducing severe theoretical and numerical complexities. Hibler (1979), on the other hand, realized that what was really needed was a simple regularization that gave sufficiently ''rigid'' behavior in the singular regime. He introduced a regularization (i.e., a ''viscous–plastic'' rheology), as described previously, in which the nonlinear viscosity of the visco–plastic rheology was bounded at a very high value such that the limiting behavior was really a very slow creep. This regularization, although simple, has its own severe numerical difficulties, which will be discussed shortly. An elastic formulation, on the other hand, has certain advantages from the numerical point of view when viewed merely as a regularization, as explained below. Thus, ironically, we are led to reintroduce a model that has some resemblance to the original AIDJEX model, but in which the regularization is a simplified elastic model whose parameters are chosen for numerical, rather than physical reasons.

The difficulty in solving (10) and (11) is primarily associated with the presence of shear strength ($\eta \neq 0$). The case $\eta = 0$ corresponds to the much simpler and easier to solve cavitating fluid model (e.g., Flato and Hibler 1992). This difficulty may be illustrated for the case of divergence-free velocity ($\nabla\cdot\mathbf{u} = 0$) and constant η and m. Setting the pressure, surface stresses, Coriolis, and tilt terms equal to $\mathbf{R}$, assumed known, the equations decouple to give

$$m\frac{\partial \mathbf{u}}{\partial t} = \eta\nabla^2\mathbf{u} + \mathbf{R}, \quad (12)$$

a simple parabolic equation. The one-dimensional stability condition for an explicit discretization of (12) is

$$\Delta t \leq \frac{m}{2\eta}\Delta x^2. \quad (13)$$

Given the maximum value of viscosity allowed in the VP model, the time step is on the order of a second for a mesh spacing of about 100 km (Ip et al. 1991) and a hundredth of a second at a resolution of about 10 km, which we anticipate in our application. This consideration led to the adoption of semi-implicit discretization schemes so that the equations could be integrated with a much less stringent time step. The solution methods currently in use are typically iterative relaxation methods (Hibler 1979; Oberhuber 1993a) whose rates of convergence scale asymptotically as $(1 - \alpha\Delta x^2)^k$ for simple test problems, where α is a positive constant and k is the number of iterations (Elman 1994). Furthermore, iterative methods are usually recursive and therefore difficult to adapt to parallel machines. There are some iterative methods, such as the conjugate gradient method, for example, whose convergence rate is linear with resolution (Elman 1994) and which can be used successfully on parallel machines (Smith et al. 1992). Use of a preconditioner further improves this method, but good preconditioners usable on parallel machines are hard to find. We will consider the use of the preconditioned conjugate gradient method later as one of the two methods studied in this paper.

Now consider a schematic hyperbolic equation of the form

$$m\frac{\partial^2 \mathbf{u}}{\partial t^2} = E\left(\nabla^2 \mathbf{u} + \frac{\mathbf{R}}{\eta}\right) + \text{damping}. \tag{14}$$

We have written (14) so that it models a damped elastic-wave mechanism that converges to the same steady-state solution as (12); E is a parameter analogous to Young's modulus. This equation is meant to represent, albeit very crudely, an elastic–plastic model of the sea ice in the regime where elastic waves dominate. The one-dimensional stability bound for an explicit discretization of (14) is

$$\Delta t \leq \sqrt{\frac{m}{E}}\Delta x, \tag{15}$$

and it is possible to arrange the stability restriction due to damping to be subsumed in (15). Thus, one might expect such an explicit scheme to converge to the steady state with a convergence rate proportional to $(1 - \alpha\Delta x)^k$, similar to that of optimum methods for parabolic equations, and much better than that of standard iterative methods. This is the rationale for considering an elastic wave adjustment process as the regularization method for the visco–plastic model in the small strain rate regime. The parameter E controls the value of the strain rate at which the regularization kicks in.

c. The elastic formulation

To construct such a model, it is usual to separate the strain rate into the sum of plastic and elastic contributions (Reuss 1930). The plastic part has already been given by (6), and the elastic part is approximated by

$$\frac{1}{E}\frac{\partial \sigma_{ij}}{\partial t} = \dot{\epsilon}_{ij}, \tag{16}$$

where E, as before, corresponds to Young's modulus. Note that this is not a physically realistic elastic equation, but one that is simplified for use as a regularization. Consistent with (1), we have neglected nonlinear advection terms. Adding the elastic and plastic contributions, we obtain

$$\frac{1}{E}\frac{\partial \sigma_{ij}}{\partial t} + \frac{1}{2\eta}\sigma_{ij} + \frac{\eta - \zeta}{4\eta\zeta}\sigma_{kk}\delta_{ij} + \frac{P}{4\zeta}\delta_{ij} = \dot{\epsilon}_{ij}. \tag{17}$$

Note that the VP rheology (6) is obtained as the steady-state limit of (17) or alternatively in the limit $E \to \infty$, while in the limit $\eta, \zeta \to \infty$ we recover the elastic equation (16). Thus, the elastic equation (16) controls the behavior in the limit of infinite viscosity, and therefore represents a regularization of the visco–plastic rheology. We also retain the limiting viscosities of Hibler (1979) in the elastic–viscous–plastic model. Although this is unnecessary, it allows more direct comparison with the VP model behavior. Equations (1) and (17) constitute the EVP model. These prognostic equations for the velocity and stress components, u_i and σ_{ij} respectively, are discretized explicitly, as described in the following section. The characteristics of this discretization are analyzed in section 4, where we obtain the appropriate choice of E and Δt to permit efficient integration while maintaining viscous–plastic balance at slow timescales.

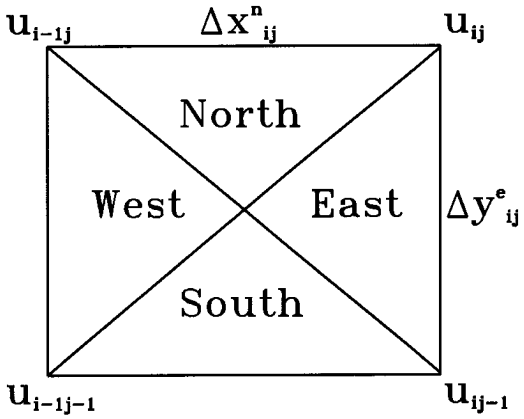

FIG. 1. Triangular regions of a grid cell. Velocity components for cell (i, j) are in the upper-right corner.

3. Numerical formulations

In this section we outline our numerical techniques for both the preconditioned conjugate gradient method and the explicit elastic–viscous–plastic method. The spatial discretization is specialized for a generalized orthogonal B-grid as in Smith et al. (1996) or Murray (1996), and each logically rectangular grid cell is divided into four triangles, as illustrated in Fig. 1. All of the thermodynamic and transport variables are given at the center of the cell, velocity is defined at the corners, and the stress tensor is constant across each triangle. We assume contravariant velocity components (velocity components aligned along grid lines). Here, σ_{ij} may take on four different values within a grid cell. This tends to avoid the grid decoupling problems associated with the B-grid. Note that the rates of strain $\dot{\epsilon}_{ij}$, and therefore the viscosities η and ζ, are also defined in each triangle. A land mask M_h is specified in the cell centers, with 0 representing land and 1 representing oceanic cells. A corresponding mask M_u for velocity and other corner quantities is given by $M_u(i, j) = \min\{M_h(l),\ l = (i, j), (i + 1, j), (i, j + 1), (i + 1, j + 1)\}$.

The velocity component equations [see (1), (5), (17), or (10), (11)] are coupled through the strain rate $\dot{\epsilon}_{ij}$, the viscosities, and the ocean stress $\boldsymbol{\tau}_w$. We lag the viscosities and c' to obtain a linear system, but leave the equations otherwise coupled.

a. Conjugate gradient solution of the viscous–plastic model

Equations (10) and (11) are discretized semi-implicitly in time as follows: if n indicates the previous time step, then

$$\alpha u^{n+1} - \partial_x[(\eta+\zeta)\partial_x u^{n+1}] - \partial_y(\eta\partial_y u^{n+1}) - \partial_x[(\zeta-\eta)\partial_y v^{n+1}] - \partial_y(\eta\partial_x v^{n+1}) = \frac{m}{\Delta t_v}u^n + \beta v^n + \tau_x - \partial_x P/2 \quad (18)$$

$$\alpha v^{n+1} - \partial_y[(\eta+\zeta)\partial_y v^{n+1}] - \partial_x(\eta\partial_x v^{n+1}) - \partial_y[(\zeta-\eta)\partial_x u^{n+1}] - \partial_x(\eta\partial_y u^{n+1}) = \frac{m}{\Delta t_v}v^n - \beta u^n + \tau_y - \partial_y P/2. \quad (19)$$

Here

$$\alpha = \frac{m}{\Delta t_v} + c'\cos\theta$$

$$\beta = mf + c'\sin\theta$$

$$\tau_x = \tau_{ai} + c'(U_w\cos\theta - V_w\sin\theta) - mg\frac{\partial H_o}{\partial x}$$

$$\tau_y = \tau_{aj} + c'(V_w\cos\theta + U_w\sin\theta) - mg\frac{\partial H_o}{\partial y}$$

$$c' = \rho_w C_w|\mathbf{U}_w - \mathbf{u}^n|.$$

All coefficients, including ζ and η, are evaluated at time level n. The viscous–plastic time step, Δt_v, is typically on the order of hours.

At time level $n+1$, spatial discretization of (18) and (19) produces a system of simultaneous equations that must be solved iteratively for the values of u^{n+1} and v^{n+1} at each grid point. The viscous–plastic rheology operator $\partial\sigma_{ij}/\partial x_j$ arises from a variational principle with the functional

$$I(u, v) = -\frac{1}{2}\iint [\eta(\partial_y u + \partial_x v)^2 + \eta(\partial_x u - \partial_y v)^2 + \zeta(\partial_x u + \partial_y v)^2]\, dx\, dy, \quad (20)$$

where η and ζ are assumed constant for the purpose of the variation in u and v, and we have temporarily ignored the pressure term. Formulas for $\partial u_i/\partial x_j$ are provided in appendix A. We discretize I, then take its variation with respect to u and v discretely to obtain the second-order derivative terms in (10) and (11). This procedure ensures that the discrete operator involved in computing $\partial\sigma/\partial x$ is both symmetric and negative definite, thereby mimicking the corresponding properties of the continuum operator. Besides providing better fidelity, these properties are highly desirable from the numerical point of view. A symmetric, negative definite operator has only negative real eigenvalues, which means that it is dissipative, ensuring nonlinear stability due to its dissipation of the total kinetic energy (Dukowicz 1997). Furthermore, symmetry is a prerequisite for some highly effective iterative solution methods, such as the conjugate gradient method to be discussed later. There is no guarantee, particularly on a nonuniform grid, that a conventional spatial discretization such as that used by Hibler will have these properties. However, on a uniform grid, the variational discretization reduces to the standard centered difference formula.

The coefficients of all "$n+1$ terms" in (18) and (19) translate into a banded matrix, which may be represented by the symmetric operator

$$\begin{bmatrix} A^TA & B \\ B^T & C^TC \end{bmatrix},$$

where

$$A^TA = -\partial_x(\zeta+\eta)\partial_x - \partial_y\eta\partial_y + \alpha$$

$$B = -\partial_y\eta\partial_x - \partial_x(\zeta-\eta)\partial_y$$

$$B^T = -\partial_x\eta\partial_y - \partial_y(\zeta-\eta)\partial_x$$

$$C^TC = -\partial_x\eta\partial_x - \partial_y(\zeta+\eta)\partial_y + \alpha.$$

The resulting matrix equation is solved iteratively with a preconditioned conjugate gradient method (Elman 1994; Ashby et al. 1990). The conjugate gradient method, along with other similar methods in its family, is particularly attractive because it is optimal among all linear iterative methods in reducing the error in a particular error norm. Because of this, it has received much attention in the literature and is being widely used, although not in the ice modeling community. The preconditioning matrix is given by

$$\begin{bmatrix} A' & 0 \\ 0 & C' \end{bmatrix},$$

where A' is the tridiagonal matrix extracted from the coefficients of A^TA, which couples the u-velocity components along a line of constant j, and C' is the corresponding tridiagonal matrix extracted from C^TC, which couples v-velocity components along a line of constant i.

Success of the method hinges on symmetry of the iterating and preconditioning matrices; for this reason we lag the terms $\pm\beta\mathbf{u}$ during the solution of (18) and (19). This treatment of the Coriolis term, which restricts the time step to about 2 hours for accuracy, might be remedied by applying a predictor–corrector method to these terms as in Zhang and Hibler (1996). This and other improvements to the VP time stepping scheme are reserved for future work.

We have employed a simple linearized Backward-Euler time discretization scheme for (18) and (19). Other methods for dealing with the nonlinearity, such as those employed by Hibler (1979) and Zhang and Hibler (1996), are somewhat more accurate but have their own difficulties. The numerical method of Hibler (1979), which we will refer to as "H79," iteratively solves the

system (10) and (11) at each time step with successive overrelaxation, utilizing a predictor–corrector method to march the equations in time. Specifically, predicted velocities at time level $n + 1/2$ are used to compute the coefficients of the linearized terms (namely, ζ, η, α, and β) before advancing to the next time level. Hibler and Ackley (1983) found a splitting problem with this procedure in cases of small nonlinear viscosities (free drift), which was corrected by a modified averaging procedure.

As with the predictor–corrector scheme, problems also arise in methods that use numerical spatial splitting and, in particular, in those methods that do not treat the entire strain rate tensor implicitly. For example, Zhang and Hibler (1996) also use successive overrelaxation to solve (10) and (11), along with a predictor–corrector time discretization scheme similar to that of Hibler (1979). In this case, however, the cross derivative terms are treated at time level n instead of $n + 1$, and the equations decouple. Then the equations for u_{ij} are solved iteratively along an entire row (i.e., constant j) before continuing to the next row, and the equations for v_{ij} are solved similarly along columns. We will refer to this method as ''ZH96.'' Stössel et al. (1994) found that treating the diagonal part of the strain rate tensor implicitly and the off-diagonal terms explicitly produced anomalous ice drifts of 6 cm s^{-1}. For the conjugate gradient method described above, the strain rate tensor remains unsplit.

b. The elastic–viscous–plastic model

Discretization in time of the momentum equation (1) is analogous to that of (18) and (19), except that the stress tensor is determined prognostically, and both (1) and (17) are subcycled with an effective EVP time step of length $\Delta t_e = \Delta t_\zeta/N$ for some integer $N > 1$ and time interval Δt_ζ. That is, N smaller time steps are taken with (1) and (17), holding η and ζ constant, for each time interval $[t_n, t_n + \Delta t_\zeta]$. Typically, $\Delta t_\zeta = \Delta t_v$, so that Δt_v is often both the viscous–plastic implicit time step and the interval at which viscosity is updated in the EVP model. Subcycling maintains the time scale on which the viscous–plastic material characteristics are changing, ensuring that the VP and EVP formulations are equivalent in the limit $\Delta t_e \to 0$, as will be seen later.

Denoting the subcycling with the index k, we time step (17) as follows, holding the viscosities constant at time level n:

$$\frac{1}{\Delta t_e}(\sigma_{ij}^{k+1} - \sigma_{ij}^{k}) + \frac{E}{2\eta}\sigma_{ij}^{k+1} + E\frac{(\eta - \zeta)}{4\eta\zeta}\sigma_{ll}^{k+1}\delta_{ij} + \frac{EP}{4\zeta}\delta_{ij} = E\dot{\epsilon}_{ij}^{k}. \quad (21)$$

(Since they both depend on the thickness variables, E and P also change on the Δt_ζ time scale, as will be seen.) This is a simultaneous equation for the three distinct stress tensor components, σ_{11}, σ_{12}, and σ_{22}, which may be inverted directly. Incidentally, we found that computing σ_{11} and σ_{22} from formulas that have the same form is important for maintaining symmetry of the numerical solutions in the x and y directions, even at some computational expense.

Given the updated stress tensor σ_{ij}^{k+1}, the momentum equation (1) is marched as follows:

$$\frac{m}{\Delta t_e}(u_i^{k+1} - u_i^k) = \frac{\partial \sigma_{ij}^{k+1}}{\partial x_j} + \tau_{ai} + c'[(U_{wi} - u_i^{k+1})\cos\theta - \varepsilon_{ij3}(U_{wj} - u_j^{k+1})\sin\theta] + \varepsilon_{ij3} m f u_j^{k+1} - mg\frac{\partial H_o}{\partial x_i}, \quad (22)$$

where $c' = \rho_w C_w|\mathbf{U}_w - \mathbf{u}^k|$. This equation may be solved for the velocity components as follows:

$$(\alpha^2 + \beta^2)u^{k+1} = \frac{m}{\Delta t_e}(\alpha u^k + \beta v^k) + \alpha\left(\frac{\partial \sigma_{1j}^{k+1}}{\partial x_j} + \tau_x\right) + \beta\left(\frac{\partial \sigma_{2j}^{k+1}}{\partial x_j} + \tau_y\right)$$

$$(\alpha^2 + \beta^2)v^{k+1} = \frac{m}{\Delta t_e}(\alpha v^k - \beta u^k) + \alpha\left(\frac{\partial \sigma_{2j}^{k+1}}{\partial x_j} + \tau_y\right) + \beta\left(\frac{\partial \sigma_{1j}^{k+1}}{\partial x_j} + \tau_x\right),$$

where $\alpha = m/\Delta t_e + c'\cos\theta$ and β, τ_x and τ_y are defined in section 3a.

The proper spatial discretization of σ_{ij} is determined analogously to the variational principle method of (20). Given formulas for $\partial u_i/\partial x_j$ provided in appendix A, we demand that in each triangle

$$\iint \left(\sigma_{ij}\frac{\partial u_i}{\partial x_j} + u_i\frac{\partial \sigma_{ij}}{\partial x_j}\right) dA = 0. \quad (23)$$

Taking the variation of (23) with respect to u_i yields formulas for the spatial derivatives of σ_{ij}. This is equivalent to the formalism used in the conjugate gradient solution of the VP model. Since Eq. (23) is another form of the variational formulation for deriving the spatial discretization, it also results in a symmetric, negative definite discrete operator, which ensures a decreasing total kinetic energy. Note that this spatial discretization is different from that in Hibler (1979).

4. Heuristic analysis of the elastic–viscous–plastic model

a. Simplified model description

The sea ice model equations are strongly nonlinear and very difficult to analyze. In this section we will consider a simplified one-dimensional version of the equations describing the EVP model in order to better understand the behavior of the model and as an aid in the selection of parameters. The simplified model assumes all spatial variation and motion occurs only in the x direction, all coefficients are constant, all forcing is absorbed into a single term τ, the constant term $P/4\zeta$ is absorbed into $\sigma = \sigma_{11}$, and $\sigma_{12} = \sigma_{22} = 0$. The model therefore is not an exact representation of the EVP model but is sufficiently similar to be useful for a heuristic analysis. The resulting equations are

$$\frac{1}{E}\frac{\partial \sigma}{\partial t} + \frac{\sigma}{\zeta} = \frac{\partial u}{\partial x} \tag{24}$$

$$m\frac{\partial u}{\partial t} = \frac{\partial \sigma}{\partial x} + \tau, \tag{25}$$

where ζ is taken to be an effective constant viscosity. The VP model is recovered in the limit $E \to \infty$:

$$m\frac{\partial u}{\partial t} = \zeta\frac{\partial^2 u}{\partial x^2} + \tau, \tag{26}$$

which will be considered as the reference for later comparisons. Conversely, in the limit $\zeta \to \infty$, (24) and (25) reduce to a purely elastic model, which supports undamped elastic waves,

$$\frac{\partial^2 u}{\partial t^2} = c_e^2\frac{\partial^2 u}{\partial x^2} + \frac{1}{m}\frac{\partial \tau}{\partial t}, \tag{27}$$

where $c_e = \sqrt{E/m}$ is the elastic wave speed. It is convenient to introduce a viscous timescale

$$T_v = \frac{m}{\zeta}\Delta x^2, \tag{28}$$

and an elastic timescale,

$$T_e = \sqrt{\frac{m}{E}}\Delta x = \frac{\Delta x}{c_e}. \tag{29}$$

As discussed in section 2, T_v is on the order of a hundredth of a second for resolutions of 10 km. In contrast, as we will see shortly, we may be allowed to choose T_e to be several orders of magnitude larger.

Equations (24)–(26) may be discretized analogously to the full set of equations given in section 3. Since the equations are linear with constant coefficients, a von Neumann stability analysis may be performed; it is outlined in appendix B for the one-dimensional EVP case described in section 5. A two-dimensional stability analysis for the complete set of equations, analogous to that given in appendix B and assuming $\Delta x = \Delta y$, is summarized in Fig. 2 in terms of the timescales (28) and (29). It is remarkable that, provided $\Delta t \le T_e\sqrt{2}$, the numerical scheme is stable irrespective of the value of the viscous timescale T_v. Had (26) been discretized explicitly, the stability limit would have been $\Delta t \le T_v/2$, implying a prohibitively small value of the time step. We will thus be able to integrate the EVP model with a time step

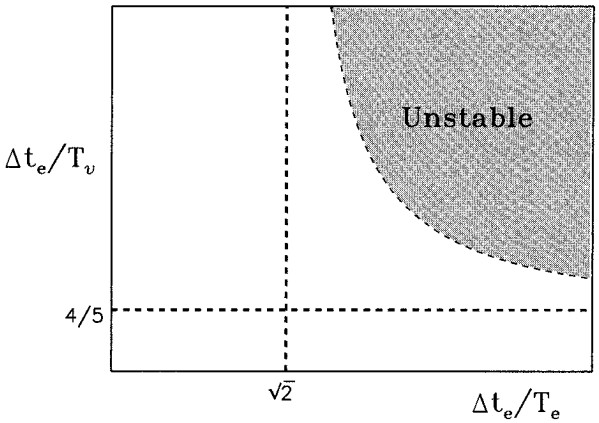

FIG. 2. Stability diagram for the 2D dynamics equations (1) and (17). Given Δx, we choose E and Δt_e so that $\Delta t_e/T_e$ lies to the left of the vertical asymptote. In this region the viscous–plastic timescale T_v is irrelevant.

$$\Delta t_e = T_e\sqrt{2}, \tag{30}$$

which is much larger than the shortest viscous timescale T_v, without resorting to implicit discretization. The time discretization of the EVP model therefore subsumes the viscous stability limit as mentioned in section 2.

In what follows it is essential to understand the effect of the time discretization and so, in the interest of simplicity, we will consider a continuous spatial representation, keeping in mind that only wavenumbers k which satisfy $k^2\Delta x^2 \le 1$ are meaningful on a grid. The time discretization of the implicit VP model is

$$\frac{m}{\Delta t_v}(u^{n+1} - u^n) = \zeta\frac{\partial^2 u^{n+1}}{\partial x^2} + \tau^n, \tag{31}$$

where u^n is the value of u at time level n, and the corresponding discretization of the EVP model is

$$\frac{1}{E\Delta t_e}(\sigma^{n+1} - \sigma^n) + \frac{\sigma^{n+1}}{\zeta} = \frac{\partial u^n}{\partial x} \tag{32}$$

$$\frac{m}{\Delta t_e}(u^{n+1} - u^n) = \frac{\partial \sigma^{n+1}}{\partial x} + \tau^n, \tag{33}$$

where Δt_e is given by (30), and

$$\frac{\Delta t_v}{\Delta t_e} = N \gg 1$$

is the number of steps, or subcycles, that the EVP model takes for each step of the VP model. One of the objectives in this section is to estimate a suitable value for

N, or in other words, to define an EVP time step Δt_e such that $\min(T_v) \ll \Delta t_e \ll \Delta t_v$. In this section, $\Delta t_\zeta = \Delta t_v$.

b. Forced response

Since (31)–(33) are linear with constant coefficients, it is possible to do a rather complete analysis. However, it is sufficient for our purposes, since the ice is forced primarily by time-varying winds, to focus on the amplitude response to periodic forcing for solutions in the form of plane waves, that is, $(u, \tau) = (\hat{u}, \hat{\tau})e^{i(kx-\omega t)}$, where ω is the angular frequency of the forcing. We characterize the response by a nondimensional parameter F,

$$F = k^2\Delta x^2 \frac{m\hat{u}}{T_v \hat{\tau}},$$

utilizing the damping factor

$$\delta = e^{-i\omega\Delta t_v} = e^{-i\omega N\Delta t_e} = \delta_e^N.$$

Here, $\delta_e = e^{-i\omega\Delta t_e}$ is the damping factor for an elastic time step Δt_e. For convenience, define $\chi = k^2\Delta x^2\Delta t_v/T_v$. Substituting plane wave solutions into the "exact" equation (26) and discretizations (31)–(33), we obtain the following response in the three cases:

Exact:

$$F = \frac{1}{1 - i\omega\Delta t_v/\chi},$$

Viscous–plastic:

$$F = \frac{1}{1 + (\delta - 1)(1 + 1/\chi)},$$

Elastic–viscous–plastic:

$$F = 1 \Bigg/ \left[1 + (\delta_e - 1)\left(\frac{N}{\chi} - \frac{T_e/T_v}{\delta_e + (\delta_e - 1)T_e/T_v}\right)\right].$$

Assuming $\omega\Delta t_e \ll 1$, the EVP response parameter becomes

$$F = 1 \Bigg/ \left[1 + (\delta_e - 1)\left(\frac{N}{\chi} - \frac{1}{T_v/T_e - i\omega\Delta t_e}\right)\right]. \quad (34)$$

We can deduce by inspection that the response in the viscous–plastic case is accurate (i.e., approximates the exact response) whenever $\delta \sim 1$, $\chi \ll 1$, and therefore the conditions for accuracy are

$$\omega\Delta t_v \ll 1 \quad (35)$$

$$k^2\Delta x^2 \frac{\Delta t_v}{T_v} \ll 1. \quad (36)$$

In the elastic–viscous–plastic case, there are two possibilities:

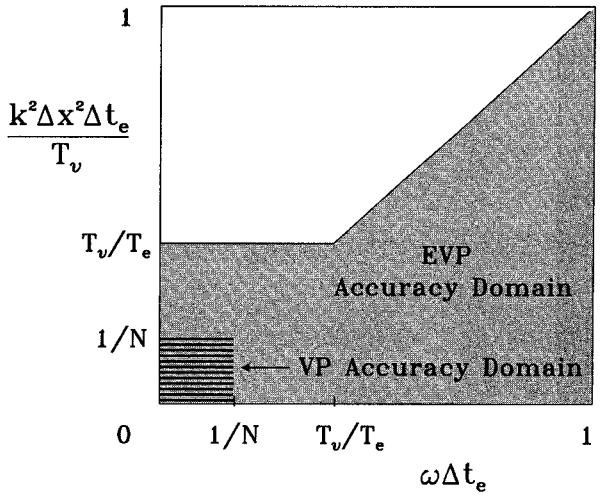

FIG. 3. Domains of accuracy of the elastic–viscous–plastic and viscous–plastic models under imposed forcing. We choose numerical parameters so that the domains are as common as possible.

$$\omega\Delta t_e \ll \frac{T_v}{T_e} \ll 1 \quad (37)$$

$$k^2\Delta x^2 \frac{\Delta t_e}{T_v}\frac{T_e}{T_v} \ll 1 \quad (38)$$

and

$$\frac{T_v}{T_e} \ll \omega\Delta t_e \ll 1 \quad (39)$$

$$\frac{k^2\Delta x^2}{\omega T_v} \ll 1. \quad (40)$$

These are consistent with the assumption made to obtain (34).

c. Choosing appropriate parameters

Conditions (35)–(40) may be more easily understood graphically. Figure 3 illustrates the domains of accuracy for the two models, using $k^2\Delta x^2\Delta t_e/T_v$ as the ordinate and $\omega\Delta t_e$ as the abscissa. In general, the EVP domain is larger than the VP domain: if $1/N < T_v/T_e$, then the VP domain is entirely contained within the EVP domain.

It is reasonable to choose parameters so that the accuracies of the two models are approximately balanced, or equivalently, that the domains of accuracy of the EVP model and the VP model are as common as possible. It is therefore desirable to have

$$\frac{\Delta t_e}{\Delta t_v} = \frac{1}{N} \approx \frac{T_v}{T_e}. \quad (41)$$

In view of (30), this is equivalent to

$$\Delta t_e^2 = T_v\Delta t_v\sqrt{2}, \quad (42)$$

and therefore E may be determined by means of (29):

$$E = \frac{\sqrt{2}m\Delta x^2}{T_v \Delta t_v}. \tag{43}$$

It is interesting that (42) implies that a suitable subcycling time step Δt_e is proportional to the harmonic average of Δt_v and the viscous timescale. This result highlights the benefits of the EVP model: the EVP time step may be orders of magnitude larger than the explicit VP time step. Since there is an entire range of viscous timescales associated with the very large range of effective viscosity coefficients, it may be appropriate to choose some intermediate value of the viscous timescale to use in estimating E. The larger the value of E one chooses, the larger the role of the elastic versus the visco–plastic strain rates and the shorter the time step Δt_e must be.

The parameter E cannot be considered a constant since then the EVP model would have dynamical effects even under free-drift conditions ($cH \to 0$) when the ice rheology should play no role. To avoid this problem, it is sufficient to assume that E has the form $E = cHE^*$ for some constant E^*. Given suitable values of T_v and $\Delta t_v(\Delta t_\zeta)$, we calculate Δt_e by (42), then calculate E for the two-dimensional problem as

$$E = \frac{2E_o \rho_i cH}{\Delta t_e^2} \min(\Delta x^2, \Delta y^2), \tag{44}$$

where $0 < E_\bigcirc < 1$. Thus, $E \to \infty$ as $\Delta t_e \to 0$, and the VP rheology (6) is obtained from the EVP formulation (17). This behavior is illustrated in Fig. 8, discussed in the following section.

5. A one-dimensional test problem

In this section we further compare the behavior of the elastic–viscous–plastic and viscous-plastic models for an essentially 1D test problem, but one which now includes nonlinear effects. Consider the more complete one-dimensional form of (1) and (17):

$$\frac{1}{E}\frac{\partial \sigma_{11}}{\partial t} + \frac{\sigma_{11}}{2\eta} + \frac{\eta - \zeta}{4\eta\zeta}(\sigma_{11} + \sigma_{22}) + \frac{P}{4\zeta} = \frac{\partial u}{\partial x} \tag{45}$$

$$\frac{1}{E}\frac{\partial \sigma_{12}}{\partial t} + \frac{\sigma_{12}}{2\eta} = 0 \tag{46}$$

$$\frac{1}{E}\frac{\partial \sigma_{22}}{\partial t} + \frac{\sigma_{22}}{2\eta} + \frac{\eta - \zeta}{4\eta\zeta}(\sigma_{11} + \sigma_{22}) + \frac{P}{4\zeta} = 0 \tag{47}$$

$$m\frac{\partial u}{\partial t} = \frac{\partial \sigma_{11}}{\partial x} + \tau, \tag{48}$$

where, as in section 4, we have lumped all forcing into τ and assumed that all motion and spatial variation occurs only in the x direction.

a. Steady state

We now consider the associated steady-state problem, which we can solve analytically with constant τ and boundary conditions $u = 0$ on the domain $0 \le x \le L$. At steady state, the stress tensor components are obtained from (45)–(47):

$$\sigma_{11} = (\zeta + \eta)\frac{\partial u}{\partial x} - \frac{P}{2} \tag{49}$$

$$\sigma_{12} = 0 \tag{50}$$

$$\sigma_{22} = (\zeta - \eta)\frac{\partial u}{\partial x} - \frac{P}{2}. \tag{51}$$

Noting that $\eta = \zeta/4$ for $e = 2$ in (49), we have

$$\sigma_{11} = \frac{5\zeta}{4}\frac{\partial u}{\partial x} - \frac{P}{2}. \tag{52}$$

Equation (48) states that

$$\frac{\partial \sigma_{11}}{\partial x} = -\tau. \tag{53}$$

Combining (52) and (53), assuming P is constant, we have

$$\frac{\partial}{\partial x}\left(\frac{5\zeta}{4}\frac{\partial u}{\partial x} + \tau x\right) = 0. \tag{54}$$

Recalling (7) and (9) and noting that the strain rate has only one component, $\dot{\epsilon}_{11} = \partial u/\partial x$, we obtain $\Delta = \sqrt{5}/4\left|\partial u/\partial x\right|$. Therefore, the viscosity ζ can have one of three possible values: $\zeta_{\min}$, $\zeta_{\max}$, and

$$P \Big/ \left(\sqrt{5}\left|\frac{\partial u}{\partial x}\right|\right). \tag{55}$$

Now, $\partial \sigma_{11}/\partial x$ cannot simultaneously be both a constant, as required by (53), and a delta function, as implied by (52) and (55); hence the solution must be composed of segments characterized by $\zeta_{\min}$ and $\zeta_{\max}$. Each segment is of the form

$$\frac{5}{4}\zeta u + \frac{1}{2}\tau x^2 + c_1 x + c_2 = 0, \tag{56}$$

where c_1, c_2 are constants. There will be three segments: two boundary segments characterized by $\zeta_{\min}$ and one in the middle characterized by $\zeta_{\max}$. We therefore have a total of six undetermined constants, plus the location of the interior break points. Boundary conditions and continuity of the solution at the two interior break points provide four constraints. Because of the lack of slope continuity at the break points, integral moments of (54) provide the additional constraints:

$$\int_0^L u^n \frac{\partial}{\partial x}\left(\frac{5\zeta}{4}\frac{\partial u}{\partial x} + \tau x\right) dx = 0,$$

where $n = 0, 1, 2, \cdots$. This closes the system.

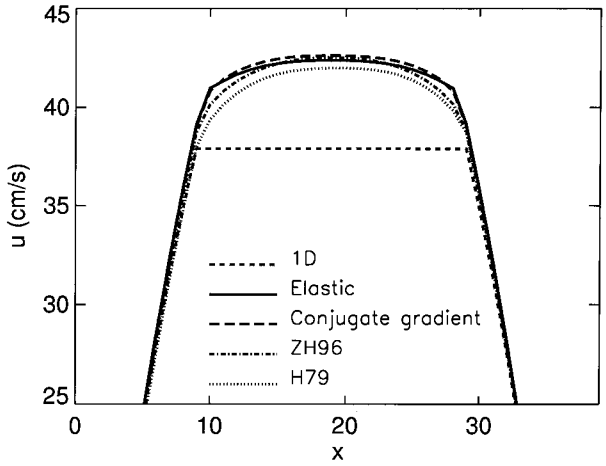

FIG. 4. Cross sections of the velocity component u produced by the (2D) viscous–plastic and elastic–viscous–plastic codes as solutions of the 1D test problem and the 1D numerical solution.

This solution is confirmed by numerical results, to be shown shortly. We now present a series of simulations that explore and compare the behavior of the EVP and VP models. Unless otherwise noted, parameter values for the simulations in this section are those given in Table 3. The 1D solution was obtained with a simple numerical code that integrates (45)–(48) to steady state.

As predicted by our analysis, the steady-state solution is composed of line segments, illustrated in Fig. 4 (labeled ''1D''). Figure 4 also presents corresponding numerical solutions of this problem from the 2D models. Due to the imposed land mask, the numerical solutions remain fundamentally two-dimensional, as illustrated in Fig. 5, and therefore not exactly comparable to the 1D solution. Implementing Neumann or periodic boundary conditions in the SOR viscous–plastic codes in order to make the solution more one-dimensional would have been time consuming and not necessary for our purposes. The four 2D models produce remarkably similar steady-state solutions.

TABLE 3. Initial values and parameters for the tests shown in Fig. 4. The error tolerance on the residual for the VP implicit schemes is given by err.

Initial values	Parameters
$c = 0.9$	$E_o = 0.25$
$H = 60.0$ cm	$\Delta t_v = 21\,600$ s
$h = 10.0$ cm	$\Delta t_\zeta = 21\,600$ s
$H_s = 10.0$ cm	$\Delta t_e = 300$ s
$h_s = 1.0$ cm	$\tau = 0.09$ g cm^{-1} s^{-2}
$\mathbf{u} = 0.0$ cm s^{-1}	err $= 10^{-5}$

The 2D equations were solved on a 40×100 grid of square cells ($\Delta x = \Delta y = 12.7$ km), and the cross sections shown are centrally located in the y direction ($j = 50$). The integration began with a uniform ice field at rest, no-slip conditions were maintained along all four boundaries, and all of the forcing terms were replaced by a single stress $\boldsymbol{\tau} = (\tau, 0)$. The CPU times shown in Table 4 represent the time used for the dynamics calculation alone; for each case, 31 s were spent in other

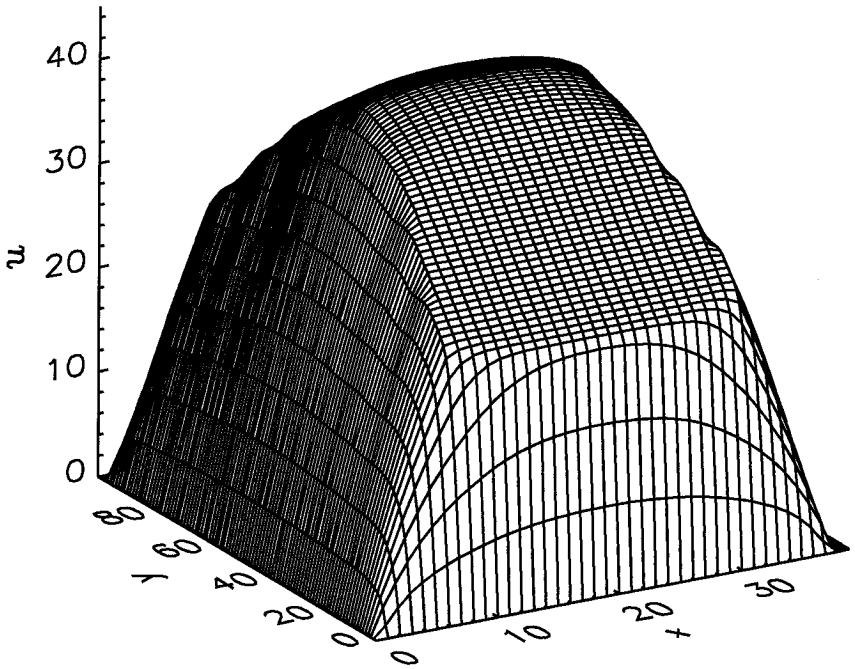

FIG. 5. Steady-state velocity component u for the 1D problem produced by the conjugate gradient VP model. The solution is inherently two-dimensional due to the boundary conditions. The cross section shown in Fig. 4 lies at $j = 50$, halfway along the y axis.

TABLE 4. Estimated total CPU times for the dynamics calculations by each of the four models and the corresponding average CPU time spent for each of the 4000 grid cells for the tests shown in Fig. 4.

Model	CPU	CPU/cell
Elastic	313 s	0.08 s
Conjugate gradient	520 s	0.13 s
ZH96	6083 s	1.52 s
H79	12 321 s	3.08 s

sections of the calculation and are not included in the table. These calculations were performed by a CRAY Y-MP8/8128 supercomputer. The models were integrated for 2700 simulated hours, taking 450 time steps with $\Delta t_\zeta = \Delta t_v = 21\,600$ s. The EVP dynamics were subcycled 72 times for each viscous–plastic time step, thus taking an effective EVP time step of length $\Delta t_e = 300$ s. The EVP numerical model is nearly 40 times more efficient than the original VP code on this test problem.

The elastic and conjugate gradient solutions shown in Figs. 4 and 5 are at steady state; the others are not. Since the corresponding EVP solution is essentially identical to Fig. 5, it is not shown. Doubling the size of the domain from 40×100 to 40×200, keeping the resolution the same, reduces the magnitude of the EVP steady-state velocity to about 38 cm s^{-1}, closely approximating the 1D numerical solution.

b. Transient behavior

We investigate the transient behavior of the EVP and VP models using two one-dimensional numerical codes, the 1D EVP code mentioned earlier and its viscous–plastic counterpart, which uses tridiagonal matrix inversion to implicitly solve the equation

$$m\frac{\partial u}{\partial t} = \frac{\partial}{\partial x}\left(\frac{5\zeta}{4}\frac{\partial u}{\partial x} - \frac{P}{2}\right) + \tau. \tag{57}$$

Both 1D models are discretized as described in section 3 for the 2D models.

Although the steady-state solutions of the VP and EVP models are the same, their transient behavior differs for typical values of Δt_v and Δt_ζ. First, consider the VP model transient behavior for different values of Δt_v, shown in Fig. 6. The very slow response of the VP model for large Δt_v is due to the linearization used in the rheology operator. If the viscosity ζ is held at time t_n during integration to time $t_{n+1} = t_n + \Delta t_v$, the linearized ice rheology operator in the viscous–plastic case (57) takes the form

$$\frac{\partial}{\partial x}\left(\zeta^n\frac{\partial u^{n+1}}{\partial x}\right).$$

Steady state is reached when $\zeta^{n+1} = \zeta^n$. Convergence of this ''outer'' iteration determines the effective time response. The adjustment process is described fully for

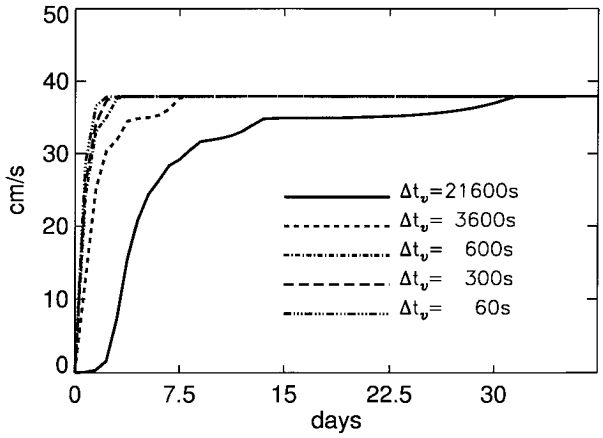

FIG. 6. Transient response of the VP model to constant surface stress for different time steps. Because of the time lag inherent in the calculation of ζ, the viscous–plastic model requires numerous time steps to reach steady state. Thus, small time steps, on the order of 10 minutes for this test problem, are necessary to obtain a converged response to an impulsively applied physical stress. Velocity at the center of the domain ($i = 20$) is shown.

this test problem in appendix C, where we determine the steady-state solution analytically and estimate the effective transition time to steady state, about 35 days for $\Delta t_v = 6$ h. Decreasing Δt_v lessens the time lag between ζ^n and $\partial u^{n+1}/\partial x$; time steps on the order of a minute produce the ''true inertial limited response'' (Hibler 1979; appendix B), illustrated in Fig. 6. That is, in order to respond accurately to an impulsively applied τ, the viscous–plastic numerical model must be integrated with a time step of 60 s or less. We refer to this solution (obtained with $\Delta t_v = 60$ s) as the reference solution.

Subcycling the EVP dynamics overcomes this difficulty somewhat. In this case, the ice rheology term has the form

$$\frac{\partial}{\partial x}\left(\zeta^n\frac{\partial u^k}{\partial x}\right),$$

where $k = 1, 2, \cdots, N$ denotes the subcycling. The improved estimates of $\partial u/\partial x$ during the VP time step improve the adjustment of the solution. When $\Delta t_\zeta = \Delta t_v$ exceeds the stability limit, as it often does, the EVP results generally lie within an envelope bounded by the viscous–plastic solutions for $\Delta t_v \to 0$ and $\Delta t_v \to \infty$, as indicated in Fig. 7.

Without subcycling, $\Delta t_e = \Delta t_\zeta$ and the elastic waves do not damp out within the viscous–plastic time step. The EVP results are then quite energetic for larger time steps, as illustrated in Fig. 8. As the time step approaches zero, however, the solutions converge to the reference solution. Furthermore, the two models produce identical results when Δt_v and Δt_ζ are much shorter than the viscous–plastic stability limit, regardless of subcycling.

Poor adjustment of the VP model has been noticed previously. Hibler (1979) remarks that the viscous–plastic rheology is slow to converge to steady state and

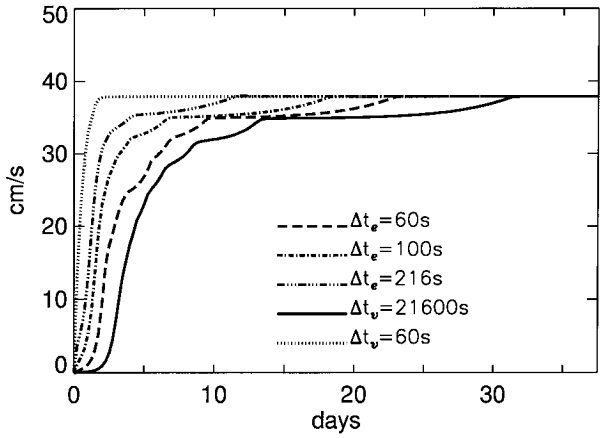

FIG. 7. Response of the EVP model as a function of Δt_e, compared to the VP model response for $\Delta t_v = 60$ s and 21 600 s. Elastic–viscous–plastic solutions $\Delta t_e = 60$ s ($N = 360$), 100 s ($N = 216$), and 216 s ($N = 100$), with viscosity updated every $\Delta t_\zeta = 21\,600$ s, all give better transient response than the viscous–plastic solution with $\Delta t_v = 21\,600$ s, but not as good as the converged viscous–plastic solutions with $\Delta t_v = 60$ s.

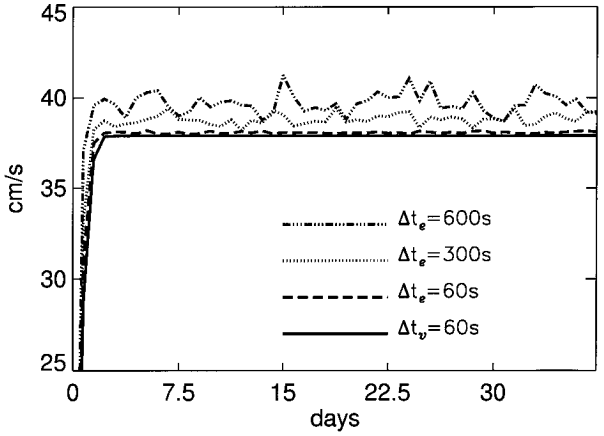

FIG. 8. Response of the EVP model without subcycling (viscosity updated on every step) as a function of time step. A substantial amount of elastic energy is excited, but the solution converges to the reference solution (solid) when $\Delta t_e = 60$ s.

requires several time steps with constant forcing to respond accurately. Similarly, Flato and Hibler (1992) note that even the cavitating fluid model should be subcycled several times without changing the forcing. However, many numerical simulations that utilize the viscous–plastic rheology, including numerous sensitivity studies, use 1-day time steps with daily varying winds (e.g., Hibler and Walsh 1982; Hibler and Ackley 1983; Walsh et al. 1985; Ip et al. 1991; Riedlinger and Preller 1991; Chapman et al. 1994). These wind stresses may vary significantly on timescales of a day or so. For example, the wind stress imposed in this example is less than 0.1 dyn cm^{-2}. Since the initial change in wind stress occurs over the first time step (6 h), this is equivalent to a change in the applied wind stress of 0.4 dyn cm^{-2} per day. The physical wind stress may vary as much as 5 dyn cm^{-2} per day (Coon 1980), an order of magnitude larger. Not surprisingly, we observe that when integrated with 1-day time steps, the VP numerical model exhibits a weak response to strongly varying winds. The improved transient behavior of the EVP model enhances its ability to capture the response of the ice to such variations in the stress. We will explore the models' responses to more realistic, time-dependent forcing in the next section.

Both the viscous–plastic transition to steady state and the magnitude of u at steady state depend on ice concentration, as shown in Fig. 9, since the maximum viscosity $\zeta_{\max}$ varies with compactness as $c\exp[c^*(1 - c)]$ through the pressure P. Because of this exponential dependence on c, P and $\zeta_{\max}$ are about two orders of magnitude less for ice concentrations of 0.8 than for 0.9, and therefore the ice rheology is immaterial for $c < 0.8$, and one cannot distinguish between elastic and viscous–plastic models.

All of the calculations reported here were done with $c = 0.9$. Holland et al. (1993) point out that shear stress becomes significant for ice concentrations greater than about 0.9. Furthermore, while open water typically exists year round throughout the Arctic, both Arctic and Antarctic ice concentrations are predominantly greater than 90% during the winter (Stössel and Claussen 1993; Gloersen et al. 1992).

6. A two-dimensional problem

As a further test, we compare the results of the numerical formulations on a geometrically simple 2D problem in which the geostrophic ocean current and wind stress terms have physically realistic magnitudes. Table 5 contains the parameter values used here. A cir-

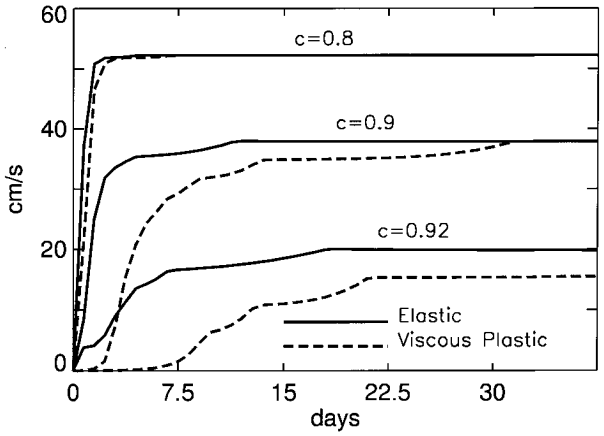

FIG. 9. Response of the EVP and VP models for different ice concentrations. While both the VP and EVP solutions exhibit appropriate transient behavior for $c \leq 0.8$, when ice rheology plays no role, the VP model response deteriorates as ice concentration increases. Velocity at the center of the domain ($i = 20$) is shown; $\Delta t_\zeta = \Delta t_v = 21600$ s and $\Delta t_e = 216$ s.

TABLE 5. Initial values and parameters for the 2D tests.

Initial values	Parameters
$c = 0.9$	$E_o = 0.25$
$H = 200.0$ cm	$\Delta t_v = 86\,400$ s
$h = 10.0$ cm	$\Delta t_\zeta = 21\,600$ s
$H_s = 10.0$ cm	$\Delta t_e = 216$ s
$h_s = 1.0$ cm	$\tau = 1.00$ g cm^{-1} s^{-2}
$\mathbf{u} = 0.0$ cm s^{-1}	err $= 10^{-6}$

cular ocean current is used that has an amplitude on the order of 10 cm s^{-1}:

$$U_x = +20(2y - L_y)/2L_y$$

$$V_y = -20(2x - L_x)/2L_x,$$

where $0 \le x \le L_x$ and $0 \le y \le L_y$. The ocean drag terms are computed as in (2). The wind stress is also specified analytically, but is based on Arctic data for the month of January 1986 provided by the Naval Research Laboratory. Fourier analysis of data in the Greenland Sea (9.2°W, 75.5°N) indicates that the characteristic timescale of the wind forcing is generally between 1 and 5 days. Based on these data, we allow the wind stress to vary 33% from a divergent stress field whose average amplitude is 3 dyn cm^{-2}, with a period $T = 4$ days:

$$\tau_i = \left[\tau \sin\left(\frac{2\pi t}{T}\right) - 3\right]\sin\left(\frac{2\pi x}{L_x}\right)\sin\left(\frac{\pi y}{L_y}\right)$$

$$\tau_j = \left[\tau \sin\left(\frac{2\pi t}{T}\right) - 3\right]\sin\left(\frac{2\pi y}{L_y}\right)\sin\left(\frac{\pi x}{L_x}\right).$$

Coriolis and ocean tilting effects have been omitted. Note that the time variation of this forcing occurs only in its magnitude. Although directional variation is not included, this (relatively quiescent) wind stress varies sufficiently to illustrate the difficulties one encounters with the VP model.

The model equations were integrated for 25 simulated days from rest with a time step $\Delta t_v = 1$ day, on a 40 $\times$ 40 grid of square cells ($\Delta x = \Delta y = 12.7$ km). Such a large time step is not feasible for the EVP dynamics model; for this case, $\Delta t_\zeta = 6$ h and $\Delta t_e = 216$ s. These time steps were chosen to illustrate the VP model's inaccuracy for conditions under which it is often used, and the improvement offered by the EVP formulation. Strictly speaking, results from the various codes are comparable only for very small Δt_v and Δt_ζ, although we observe in Figs. 10 and 11 that the values of Δt_v and Δt_ζ used here are sufficiently small to produce comparable results.

These results differ slightly from a time-accurate reference solution, which we define as that produced by the conjugate gradient method with a time step of 60 s. In Fig. 12, we present the differences of domain-averaged kinetic energies per unit mass for each of the methods with that of the reference solution. This comparison indicates that while all of the methods reach a quasi-steady state, the EVP model is much more accurate during the initial ''spin up'' from rest, and suggests that the EVP model will behave significantly better under the severe wind forcing conditions observed in the polar regions. For example, Arctic winds have been observed to change as much as 350% in a three-day period (Reyn-

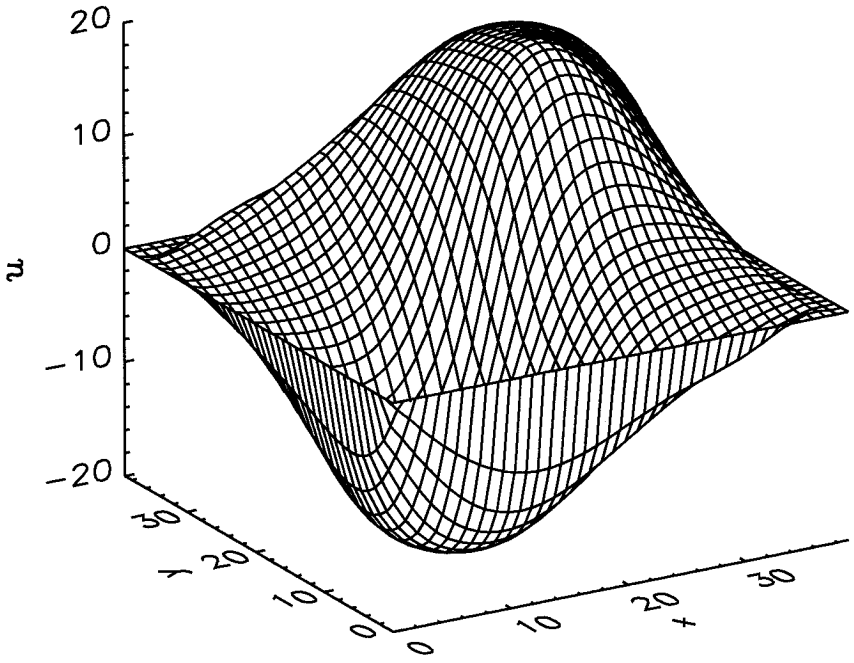

FIG. 10. The VP velocity component u for the 2D test case at $t = 25$ days, produced with the H79 numerical model.

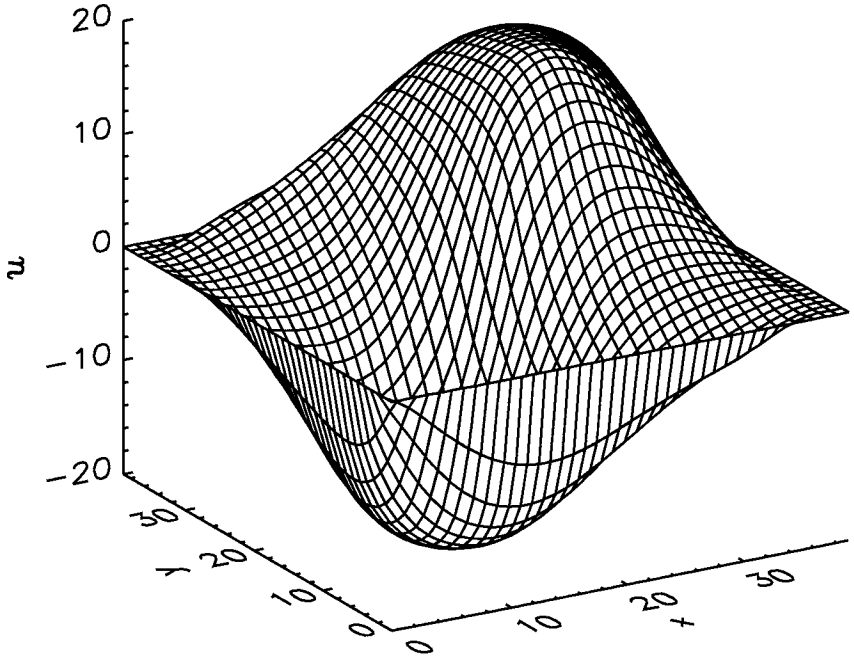

FIG. 11. The EVP velocity component u for the 2D test case at $t = 25$ days. Comparison with the corresponding VP solution in Fig. 10 shows that the EVP model produces solutions equivalent to those of the VP model and validates the 1D results of sections 4 and 5.

olds 1984), and the ice edge may move 35 km day^{-1} under gale conditions (Roed and O'Brien 1983). In general, geostrophic winds are responsible for 60%–80% of the daily ice variance (Serreze et al. 1989). On these timescales, it is essential that a numerical model for ice dynamics respond accurately to the imposed forcing.

Furthermore, the magnitude of the differences between the viscous–plastic model solutions and the reference case in Fig. 12 indicate that the VP models are slow to respond to more typical forcing variations. The kinetic energy of the H79 solution is better than the conjugate gradient solution by about a factor of 2 due to effectively two iterations of the linearization being taken in the predictor–corrector method used for the time stepping. Incorporating a predictor–corrector method into the time discretization of the conjugate gradient numerical model would improve its accuracy to that of the H79 model, but degrade its efficiency. Regardless, neither VP model is as accurate as the EVP model.

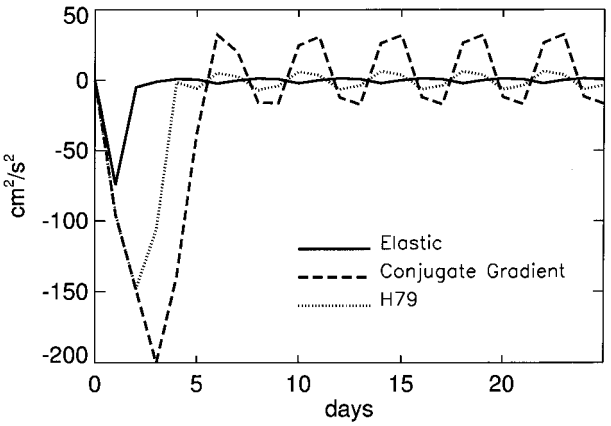

FIG. 12. The difference between the domain-averaged kinetic energy per unit mass of the elastic, conjugate gradient, and H79 methods computed with $\Delta t_v = 1$ day and the domain-averaged kinetic energy per unit mass of the conjugate gradient solution computed with $\Delta t_v = 60$ s (the reference solution). For the elastic solution, $\Delta t_\zeta = 6$ h and $\Delta t_e = 216$ s. The viscous–plastic models require 4 days to reach a quasi-steady state, after which their response to the variable forcing tends to lag behind the exact response.

The CPU times given in Table 6 represent the time used for the dynamics calculation alone; the 4 s spent performing I/O for each case is not included in the table. Implementing a two-step time discretization scheme for the conjugate gradient VP numerical model would improve its forcing response to roughly the level of the H79 code and slow it down by approximately a factor of 2. Note that for the $\Delta t_v = 60$ s calculation, the conjugate gradient dynamics used 1379 s CPU. We have not made the corresponding calculation with the H79 method, but based on the figures in Table 6, the H79

TABLE 6. Estimated total CPU times for the 2D tests by each of the models and the corresponding average CPU time spent for each of the 1600 grid cells.

Model	CPU	CPU/cell
Elastic	41 s	0.026 s
Conjugate gradient	9 s	0.006 s
H79	107 s	0.067 s

model would have taken about 12 times longer, or 4.5 h, to perform this calculation. Thus, the standard VP model would require several CPU hours to reach the level of accuracy obtained with $\Delta t_v = 60$ s, which the EVP model simulates fairly well in only 41 CPU seconds using $\Delta t_\zeta = 6$ h and $\Delta t_e = 216$ s.

7. Summary

Despite its physical and computational problems, the nonlinear viscous–plastic rheology proposed by Hibler (1979) is the most widely accepted model for sea ice dynamics. In the model's physical description, the ice viscosity suffers a severe singularity: treated as a viscous fluid, rigid sea ice has infinite viscosity. Hibler regularized this problem by setting a maximum viscosity bound, thereby allowing the ice to creep slowly rather than being completely rigid. Even so, the viscosity ranges over many orders of magnitude, and integrating the implicit VP numerical model requires large computational resources, particularly for high resolution grids on parallel architectures. Using smaller maximum viscosity values increases the model's computational efficiency but produces less accurate results. Our explicit elastic–viscous–plastic model utilizes an elastic mechanism in regions of rigid ice to significantly increase the computational efficiency of the VP numerical model. For comparison purposes, we have chosen to retain the maximum viscosity bound for the results presented here. In this paper we also present a fast, though still implicit, conjugate gradient method for solving the VP equations. Although the conjugate gradient method's efficiency is comparable to the EVP method's on serial machines, the explicit EVP model will be substantially more efficient on parallel computers.

Furthermore, due to its semi-implicit treatment of the ice rheology, the standard numerical formulation of the VP model has very poor time response for time steps typically used by researchers in the field, which are often as long as a day. Our investigation of a simplified, one-dimensional version of the VP model indicates that the viscous–plastic model behavior is acceptable only for wind stresses that vary slowly. However, for wind stresses that vary significantly on timescales of a day, the viscous–plastic model response is weak.

This computational pathology may be resolved by improving the numerical method or by changing the physical parameterization in the model. The EVP model represents a combination of these approaches: its (albeit nonphysical) elastic waves enable the use of an efficient, explicit numerical method. We observe improved transient behavior of the solutions, enhancing the model's ability to capture the ice response to variations in the imposed stress. However, because the EVP model is based on the same linearized viscous–plastic rheology as the VP model, it may inherit similar problems in some parameter regimes.

We have shown that a large range of the elastic wave parameter E exists for which the EVP numerical method is both stable and efficient. In particular, this allows the elastic time step to be orders of magnitude larger than the viscous–plastic timescale in areas of rigid ice. Several considerations must be weighed when choosing the model parameters. The timescale of the external forcing places an upper bound on Δt_v or Δt_ζ. The choice of the subcycling time step Δt_e is based on considerations of efficiency and accuracy; some guidelines for choosing Δt_e are given in section 4. The parameter values used in this paper, namely for Δt_ζ, E, and Δt_e, are representive of suitable values that improve both the numerical efficiency and accuracy of the viscous–plastic ice model. A more complete parameter sensitivity study will be reported later.

Other numerical concerns involve maintaining operator symmetry and energy dissipation properties in the discretization of the stress tensor, which arises from a variational principle. Dividing the grid cells into four triangles for spatial discretizations results in higher resolution of the stress tensor and viscosity fields than of thickness and velocity. These numerical improvements, along with the formulation of the EVP model, have resulted in a fast, efficient model of sea ice dynamics well suited to climate studies on parallel machines.

We have coupled the EVP dynamics model to thermodynamic and transport components and will be testing this ice model with daily atmospheric fluxes and validating it with remotely sensed and in situ observations. More complete descriptions of the thermodynamics and transport components and results from the validation of the complete sea ice model are forthcoming.

Acknowledgments. We wish to thank A. Semtner for providing the ZH96 code, M. Maltrud and C. A. Lai for Arctic datasets, and A. Hagberg for many helpful discussions. We are grateful to S. Piacsek for providing Arctic wind stress data and comments on the manuscript. This work has been supported by the DOE CHAMMP Program. We also thank the Center for Nonlinear Studies and the DOE HPCC-NLS program for technical support.

APPENDIX A

Numerical Formulations

Formulas for the spatial derivatives of a field A_{ij}, defined at the upper-right corner of the grid cell (see Fig. 1), are given below. Δx^c_{ij} and Δy^c_{ij} are midcell lengths. Assuming the field A is linear in x and y within each triangle,

North:

$$\frac{\partial A}{\partial x} = \frac{A_{ij} - A_{i-1j}}{\Delta x^n_{ij}}$$

$$\frac{\partial A}{\partial y} = \frac{A_{ij} + A_{i-1j} - A_{ij-1} - A_{i-1j-1}}{2\Delta y^c_{ij}}$$

East:

$$\frac{\partial A}{\partial x} = \frac{A_{ij} + A_{ij-1} - A_{i-1j} - A_{i-1j-1}}{2\Delta x^c_{ij}}$$

$$\frac{\partial A}{\partial y} = \frac{A_{ij} - A_{ij-1}}{\Delta y^c_{ij}}$$

South:

$$\frac{\partial A}{\partial x} = \frac{A_{ij-1} - A_{i-1j-1}}{\Delta x^n_{ij-1}}$$

$$\frac{\partial A}{\partial y} = \frac{A_{ij} + A_{i-1j} - A_{ij-1} - A_{i-1j-1}}{2\Delta y^c_{ij}}$$

West:

$$\frac{\partial A}{\partial x} = \frac{A_{ij} + A_{ij-1} - A_{i-1j} - A_{i-1j-1}}{2\Delta x^c_{ij}}$$

$$\frac{\partial A}{\partial y} = \frac{A_{i-1j} - A_{i-1j-1}}{2\Delta y^e_{i-1j}}.$$

APPENDIX B

Stability of the 1D Equations

We perform a von Neumann stability analysis of the simplified, 1D dynamics equations (45)–(48). Discretizing time, these equations become

$$\frac{m}{\Delta t}(u^{n+1} - u^n) - \frac{\partial \sigma^{n+1}}{\partial x} = 0$$

$$\frac{1}{E\Delta t}(\sigma^{n+1} - \sigma^n) + \frac{5\sigma^{n+1}}{4\zeta} - \frac{25}{16}\frac{\partial u^n}{\partial x} = 0.$$

Assume that both u and σ have the form $a^n e^{ijk\Delta x}$, and $a^{n+1} = \lambda a^n$. Then the characteristic equation is

$$\lambda^2 (1 + \alpha) + \lambda (-2 - \alpha + k^2\beta) + 1 = 0,$$

where $\alpha = 5E\Delta t/4\zeta$ and $\beta = 25E\Delta t^2/16m$. Solutions are stable whenever $|\lambda| < 1$, that is, for

$$\alpha > \frac{1}{2}k^2\beta - 2.$$

Let $\xi = \Delta t/T_e$ and $\gamma = \Delta t/T_v$, then $\gamma = 4\beta/5\alpha\Delta x^2$ and the boundary of the stability region is given by the hyperbolic function

$$\gamma = 10\xi^2 \Big/ \left(\frac{25}{4}\xi^2 k^2 \Delta x^2 - 16\right).$$

The stability region of the 2D equations, shown in Fig. 2, is similar.

APPENDIX C

VP Model Adjustment to Imposed Forcing

The VP adjustment time illustrated in Fig. 6 for time steps of 6 h or more may be estimated as follows. For large time steps, the acceleration term may be neglected, and the transient iterates of the resulting numerical scheme approximate the transition to steady state. That is, we integrate (54) over $[x, L/2]$ and take advantage of the problem's symmetry about $x = L/2$ to produce the relation

$$\zeta\frac{\partial u}{\partial x} = \frac{4}{5}\tau\left(\frac{L}{2} - x\right).$$

The transition to steady state is then governed by the associated iterative scheme,

$$\frac{\partial u^{n+1}}{\partial x} = \begin{cases} GP'/\zeta_{\max} & \text{if } \zeta > \zeta_{\max} \\ G\left|\dfrac{\partial u^n}{\partial x}\right| & \text{if } \zeta_{\min} < \zeta < \zeta_{\max} \\ GP'/\zeta_{\min} & \text{if } \zeta < \zeta_{\min}, \end{cases} \tag{C1}$$

where $P' = P/\sqrt{5}$, (55) has been incorporated for ζ and

$$G = \frac{4\tau}{\sqrt{5}P}\left(\frac{L}{2} - x\right). \tag{C2}$$

Thus, the upper and lower bounds imposed on ζ now limit $\partial u/\partial x$. The iteration begins with $u = 0$ and $\zeta = \zeta_{\max}$ for all x. Recall that the steady-state solution is composed of three line segments, the inner section characterized by $\zeta_{\max}$ and the two outer sections by $\zeta_{\min}$. In the inner section, ζ will remain equal to $\zeta_{\max}$, but in the outer regions, ζ, given by (55), will change from $\zeta_{\max}$

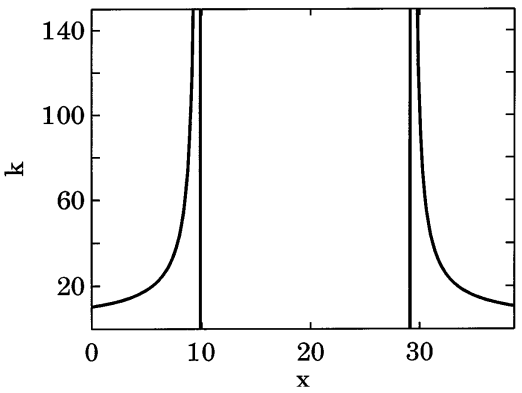

FIG. C1. The number of iterations, k, needed for ζ to change from $\zeta_{\max}$ to $\zeta_{\min}$, as a function of x. The vertical lines indicate the break points, between which $\zeta = \zeta_{\max}$. The number of steps required for the solution to reach steady state is given approximately by the largest value of k at the grid points nearest the break points, about 140 in this case.

to $\zeta_{\min}$. Equivalently, $|\partial u/\partial x|$ will change from $|\partial u/\partial x|_{\max}$ to $|\partial u/\partial x|_{\min}$, under the iteration (C1). Let k be the number of iterations for this change to occur; then

$$|G|^k \left|\frac{\partial u}{\partial x}\right|_{\min} = \left|\frac{\partial u}{\partial x}\right|_{\max}.$$

In general, k will be a function of x. For this test case, $|\partial u/\partial x|_{\max} = 2.2 \times 10^{-6}$ and $|\partial u/\partial x|_{\min} = 1.8 \times 10^{-9}$ (for $P = 2 \times 10^6$) so that

$$k = \frac{\ln 1.2 \times 10^3}{\ln|G|}, \tag{C3}$$

illustrated in Fig. C1. This formula is valid only in the outer regions and fails at the break points, where $|G| = 1$:

$$x = \frac{L}{2} \pm \frac{\sqrt{5}P}{4\tau}.$$

Here, k is largest for the grid points nearest the inner region; this analysis suggests that approximately 140 iterations are needed for the solution to reach steady state, in good agreement with Fig. 6.

REFERENCES

Ashby, S. F., T. A. Manteufel, and P. E. Saylor, 1990: A taxonomy for conjugate gradient methods. *SIAM J. Numer. Anal.,* **27,** 1542–1568.

Bratchie, I., 1984: Rheology of an ice-floe field. *Ann. Glaciol.,* **5,** 23–28.

Bryan, K., S. Manabe, and R. L. Pacanowski, 1975: A global ocean–atmosphere climate model. Part II: The oceanic circulation. *J. Phys. Oceanogr.,* **5,** 30–46.

Campbell, W. J., 1965: The wind-driven circulation of ice and water in a polar ocean. *J. Geophys. Res.,* **70,** 3279–3301.

Chapman, W. L., W. J. Welch, K. P. Bowman, J. Sacks, and J. E. Walsh, 1994: Arctic sea ice variability: Model sensitivities and a multidecadal simulation. *J. Geophys. Res.,* **99,** 919–935.

Colony, R., and R. S. Pritchard, 1975: Integration of elastic–plastic constitutive laws. *AIDJEX Bull.,* **30,** 55–80.

Coon, M. D., 1980: A review of AIDJEX modeling. *Sea Ice Processes and Models,* R. S. Pritchard, Ed., University of Washington Press, 12–25.

——, S. A. Maykut, R. S. Pritchard, D. A. Rothrock, and A. S. Thorndike, 1974: Modeling the pack ice as an elastic-plastic material. *AIDJEX Bull.,* **24,** 1–105.

Dukowicz, J. K., 1997: Comments on ''Stability of the viscous–plastic sea ice rheology.'' *J. Phys. Oceanogr.,* **27,** 480–481.

——, R. D. Smith, and R. C. Malone, 1993: A reformulation and implementation of the Bryan–Cox–Semtner ocean model on the connection machine. *J. Atmos. Oceanic Technol.,* **10,** 195–208.

——, ——, and ——, 1994: Implicit free-surface method for the Bryan–Cox–Semtner ocean model. *J. Geophys. Res.,* **99,** 7991–8014.

Elman, H. C., 1994: Iterative methods for linear systems. *Large-Scale Matrix Problems and the Numerical Solution of Partial Differential Equations,* J. Gilbert and D. Kershaw, Eds., *Advances in Numerical Analysis,* Vol. III, Clarendon Press, 69–177.

Felzenbaum, A. I., 1961: The theory of steady drift of ice and the calculation of the long period mean drift in the central part of the Arctic Basin. *Probl. North,* **2,** 13–44. [Originally in *Problemy Severa,* No.2, pp. 16–46, 1958.]

Flato, G. M., and W. D. Hibler III, 1989: On a simple sea-ice dynamics model for climate studies. *Ann. Glaciol.,* **14,** 72–77.

——, and ——, 1990: A cavitating fluid sea ice model. *Cold Reg. Res. Eng. Lab. Monogr.,* No. 90-1,

——, and ——, 1992: Modeling pack ice as a cavitating fluid. *J. Phys. Oceanogr.,* **22,** 626–651.

Gloersen, P., W. J. Campbell, D. J. Cavalieri, J. C. Comiso, C. L. Parkinson, and H. J. Zwally, 1992: Arctic and Antarctic sea ice, 1978–1987: Satellite passive-microwave observations and analysis. NASA Tech. Rep. SP-511, 290 pp. [Available from Laboratory for Hydrospheric Processes, NASA Goddard Space Flight Center, Greenbelt, MD 20771.]

Gray, J. M. N. T., and L. W. Morland, 1994: A two-dimensional model for the dynamics of sea ice. *Philos. Trans. Roy. Soc. London A,* **347,** 219–290.

Hibler, W. D., III, 1974: Differential sea ice drift II: Comparison of mesoscale strain measurements to linear drift theory predictions. *J. Glaciol.,* **13,** 457–471.

——, 1979: A dynamic thermodynamic sea ice model. *J. Phys. Oceanogr.,* **9,** 817–846.

——, 1980: Modeling a variable thickness sea ice cover. *Mon. Wea. Rev.,* **108,** 1943–1973.

——, 1986: Ice dynamics. chap. 9, *The Geophysics of Sea Ice,* N. Untersteiner, Ed., *NATO ASI Series B: Physics,* Plenum Press, 577–640.

——, and W. B. Tucker III, 1979: Some results from a linear viscous model of the Arctic ice cover. *J. Glaciol.,* **22,** 293–304.

——, and J. E. Walsh, 1982: On modeling seasonal and interannual fluctuation of Arctic sea ice. *J. Phys. Oceanogr.,* **12,** 1514–1523.

——, and S. F. Ackley, 1983: Numerical simulation of the Weddell Sea pack ice. *J. Geophys. Res.,* **88,** 2873–2887.

——, and K. Bryan, 1987: A diagnostic ice–ocean model. *J. Phys. Oceanogr.,* **17,** 987–1015.

Holland, D. M., L. A. Mysak, D. K. Manak, and J. M. Oberhuber, 1993: Sensitivity study of a dynamic thermodynamic sea ice model. *J. Geophys. Res.,* **98,** 2561–2586.

Ip, C. F., W. D. Hibler III, and G. M. Flato, 1991: On the effect of rheology on seasonal sea ice simulations. *Ann. Glaciol.,* **15,** 17–25.

Manabe, S., K. Bryan, and M. J. Spelman, 1979: A global ocean–atmosphere climate model with seasonal variation for future studies of climate sensitivity. *Dyn. Atmos. Oceans,* **3,** 393–426.

Murray, R. J., 1996: Explicit generation of orthogonal grids for ocean models. *J. Comput. Phys.,* **126,** 251–273.

Nikiforov, Y. G., A. M. Gukovich, Y. N. Yefimov, and M. A. Romanov, 1967: Principles of a method for calculating the ice redistribution under the influence of the wind during the navigation period in the Arctic seas. *AIDJEX Bull.,* **3,** 40–64. [Originally in *Tr. Arkt. Antarkt. Inst.,* **257,** pp. 5–25, 1967.]

Oberhuber, J. M., 1993a: Simulation of the Atlantic circulation with a coupled sea ice–mixed layer–isopycnal general circulation model. Part I: Model description. *J. Phys. Oceanogr.,* **23,** 808–829.

——, 1993b: Simulation of the Atlantic circulation with a coupled sea ice–mixed layer–isopycnal general circulation model. Part II: Model experiment. *J. Phys. Oceanogr.,* **23,** 830–845.

Parkinson, C. L., and W. M. Washington, 1979: A large-scale numerical model of sea ice. *J. Geophys. Res.,* **84,** 311–337.

Pritchard, R. S., 1975: An elastic-plastic constitutive law for sea ice. *J. Appl. Mech.,* **42E,** 379–384.

——, M. D. Coon, and M. G. McPhee, 1977: Simulation of sea ice dynamics during AIDJEX. *J. Pressure Vessel Tech.,* **99J,** 491–497.

Reuss, A., 1930: Berucksichtigung der elastischen formanderung in der plastizitats theorie. *Z. Ang. Math. Mech.,* **10,** 266.

Reynolds, M., 1984: On the local meteorology at the marginal ice zone of the Bering Sea. *J. Geophys. Res.*, **89,** 6515–6524.

Riedlinger, S. H., and R. H. Preller, 1991: The development of a coupled ice-ocean model for forecasting ice conditions in the Arctic. *J. Geophys. Res.*, **96,** 16 955–16 977.

Roed, L. P., and J. J. O'Brien, 1983: A coupled ice-ocean model of upwelling in the marginal ice zone. *J. Geophys. Res.*, **88,** 2863–2872.

Rothrock, D. A., 1975a: The steady drift of an incompressible Arctic ice cover. *J. Geophys. Res.*, **80,** 387–397.

——, 1975b: The energetics of the plastic deformation of pack ice by ridging. *J. Geophys. Res.*, **80,** 4514–4519.

Serreze, M. C., R. G. Barry, and A. S. McLaren, 1989: Seasonal variations in sea ice motion and effects on sea ice concentration in the Canada Basin. *J. Geophys. Res.*, **94,** 10 955–10 970.

Smith, R. D., J. K. Dukowicz, and R. C. Malone, 1992: Parallel ocean general circulation modeling. *Physica D,* **60,** 38–61.

——, S. Kortas, and B. Meltz, 1997: Curvilinear coordinates for global ocean models. *J. Comput. Phys.*, in press.

Stössel, A., and M. Claussen, 1993: On the momentum forcing of a large-scale sea-ice model. *Climate Dyn.*, **9,** 71–80.

——, J. M. Oberhuber, and E. Maier-Reimer, 1994: Sensitivites of the sea-ice component of two ocean general circulation models. Max-Plank-Institut für Meteorologie, Hamburg, Tech. Rep. 138, 44 pp. [Available from Max-Planck-Institute Für Meteorologie, Bundesstrasse 55, 20146 Hamburg, Germany.]

Walsh, J. E., W. D. Hibler III, and B. Ross, 1985: Numerical simulation of Northern Hemisphere sea ice variability, 1951–1980. *J. Geophys. Res.*, **90,** 4847–4865.

Warn-Varnas, A., R. Allard, and S. Piacsek, 1991: Synoptic and seasonal variations of the ice-ocean circulation in the Arctic: A numerical study. *Ann. Glaciol.*, **15,** 54–62.

Zhang, J., and W. D. Hibler, 1996: On an efficient numerical method for modeling sea ice dynamics. *J. Geophys. Res.*, in press.